Combining Single RNA Sensitive Probes with Subdiffraction-Limited and Live-Cell Imaging Enables the Characterization of Virus Dynamics in Cells

Eric Alonas,[†] Aaron W. Lifland,[‡] Manasa Gudheti,[‡] Daryll Vanover,[†] Jeenah Jung,[†] Chiara Zurla,[†] Jonathan Kirschman,[†] Vincent F. Fiore,[†] Alison Douglas,[†] Thomas H. Barker,[†] Hong Yi,[§] Elizabeth R. Wright,[§,⊥] James E. Crowe, Jr.,[∥,#] and Philip J. Santangelo[†,*]

[†]Wallace H. Coulter Department of Biomedical Engineering, Georgia Institute of Technology and Emory University, 313 Ferst Drive, UA Whitaker Bldg, Atlanta, Georgia 30332, United States, [‡]Vutara, Inc., 615 Arapeen #304, Salt Lake City, Utah 84108, United States, [§]Robert P. Apkarian Integrated Electron Microscopy Core, College of Medicine, Emory University, Atlanta, Georgia 30322, United States, [⊥]Department of Pediatrics, Division of Infectious Diseases, Emory University School of Medicine, 2015 Uppergate Drive, NE, Suite 548, Atlanta, Georgia 30322, United States, [∥]Department of Pediatrics, Vanderbilt University School of Medicine, Nashville, Tennessee 37232, United States, and [#]Department of Pathology, Microbiology and Immunology, Vanderbilt University School of Medicine, Nashville, Tennessee 37232, United States. E.A. and P.J.S. designed the experiments. E.A. performed the experiments and wrote the manuscript. A.W.L. and M.G. performed the dSTORM imaging. V.F.F., A.D., and T.H.B. provided the fibronectin micropatterned dishes. E.A., H.Y., and E.R.W. prepared and imaged TEM samples. E.A., A.W.L., D.V., J.J., C.Z., J.K., J.E.C., and P.J.S. edited the manuscript.

ABSTRACT The creation of fluorescently labeled viruses is currently limited by the length of imaging observation time (*e.g.*, labeling an envelope protein) and the rescue of viral infectivity (*e.g.*, encoding a GFP protein). Using single molecule sensitive RNA hybridization probes delivered to the cytoplasm of infected cells, we were able to isolate individual, infectious, fluorescently labeled human respiratory syncytial virus virions. This was achieved without affecting viral mRNA expression, viral protein expression, or infectivity. Measurements included the characterization of viral proteins and genomic RNA in a single virion using dSTORM, the development of a GFP fusion assay, and the development of a pulse-chase assay for viral RNA production that allowed for the detection of both initial viral RNA and nascent RNA production at designated times postinfection. Live-cell measurements included imaging and characterization of filamentous virion fusion and the quantification of virus replication within the same cell over an eight-hour period. Using probe-labeled viruses, individual viral particles can be characterized at subdiffraction-limited resolution, and viral infections can be quantified in single cells over an entire cycle of replication. The implication of this development is that MTRIP labeling of viral RNA during virus assembly has the potential to become a general methodology for the labeling and study of many important RNA viruses.

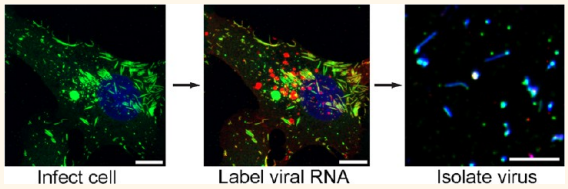

KEYWORDS: respiratory syncytial virus · live-cell imaging · fluorescent virus tracking · fusion · replication · nanoscopy

Valuable information about the infection life-cycle of a virus can be obtained by imaging single virions infecting live cells. Such studies can elucidate mechanisms of attachment (*e.g.*, virus surfing[1]), cellular entry (*e.g.*, endocytosis[2−5]) or egress (*e.g.*, viral protein accumulation[6,7]), and associated host cell factors[8,9] on a single-cell basis in real time. Several methods have been used previously to label viruses, including the introduction of lipophilic fluorescent dyes to label viral envelopes;[3−5,8−13] covalently bound organic fluorophores[2,4,13−15] or recombinant GFP fusion proteins[1,6,7,16] to label viral structural proteins; and nucleic acid specific dyes[2] or RNA hairpin-recognizing, GFP fusion proteins[7] to label viral genomic molecules. However, methods that label viral envelopes or virion surface proteins can be used only to visualize viral attachment, early entry, or late assembly. Once the viral ribonucleoprotein (RNP) dissociates from the labeled envelope, virus replication can no longer be observed with such protein labels. RNA-specific dyes might diffuse toward other cellular RNAs if not confined to the viral capsid space. Additionally, the use of

* Address correspondence to philip.santangelo@bme.gatech.edu.

Received for review August 3, 2013 and accepted December 18, 2013.

Published online December 18, 2013
10.1021/nn405998v

recombinant viruses often is limited by the adverse effects of modifications on viral replication and assembly. This is due to the large number of inserted nucleotides required for labeling, which are often a significant percentage of the total length of the resulting construct. Conventional methods are useful for elucidating certain aspects of viral processes, but they do not allow for the long-term imaging of viral genome entry and replication in cell culture.

In this article, we present a new method for labeling RNA viruses using multiply labeled tetravalent RNA imaging probes (MTRIPs). These probes consist of a chimeric DNA/2′-*O*-methyl RNA oligonucleotide labeled internally with fluorophores and tetravalently complexed to neutravidin by a 5′ biotin modification.[17] We demonstrate the usefulness of the method through the targeting of the intergenic-gene start regions of the human respiratory syncytial virus (hRSV) genomic RNA (gRNA). hRSV was used as a model virus for this method because only a few recombinant fluorescent versions of the virus have been successfully created[18,19] and conventional methods of virion labeling cannot be applied easily. hRSV is pleomorphic, producing both spherical-like and filamentous virions that vary in size from ~100 nm to 10 μm.[20] This phenomenon makes identifying infectious particles upon first inspection difficult. In addition, the entry and replication of filamentous hRSV virions has not been studied extensively using live-cell imaging,[21,22] and the study of filamentous virion particles is relevant not only to hRSV but other highly pathogenic RNA viruses, such as Ebola and influenza.

Here, we demonstrate the ability to label the gRNA of hRSV in filamentous and spherical-like virions successfully using MTRIPs. We demonstrate that MTRIP-labeled hRSV virions could be isolated on glass coverslips, stained for viral proteins, and interrogated using both diffraction-limited deconvolution microscopy and the subdiffraction resolution method direct stochastic optical reconstruction microscopy (dSTORM). Using deconvolution microscopy, the co-localization of gRNA with the viral nucleoprotein (N) and viral fusion protein (F) was used to identify virions and determine a rapid estimate of virus titer of infectious particles. Using dSTORM, a more accurate image of the virion morphology was obtained. Next, we showed that MTRIP-labeled virions were infectious, producing new gRNA and viral proteins, and could be used to identify cells that were infected only one hour after inoculation, as opposed to the 24 h needed for a traditional GFP-based assay. Additionally, we analyzed the motion of the gRNA from a filamentous virion during cell entry, which exhibited dynamic characteristics largely of passive transport punctuated by occasional evidence of active transport. We provide additional evidence that this motion was due to virion fusion and not endocytosis. Lastly, we demonstrate that MTRIP-labeled virions could be used to collect single-cell statistics on viral gRNA replication over the course of an eight-hour infection. This technique provides a general live-cell method that can be applied broadly to other RNA viruses to study their dynamics and replication over biologically relevant time periods.

RESULTS AND DISCUSSION

Characterization of MTRIP-Labeled Filamentous Virions. A brief description of the method is shown in Figure 1. Briefly, MTRIPs were assembled by incubating biotinylated, fluorescently labeled oligonucleotides with neutravidin, and excess oligonucleotides were removed by filtration[17] (Figure 1A). These MTRIPs, which bind *via* Watson−Crick base-pairing to a short, repeated sequence within the intergenic-gene start regions of the hRSV genome, were delivered into hRSV-infected cells (Figure 1B) *via* reversible streptolysin-O permeabilization, a pore-forming toxin of *Streptococcus pyogenes* (Figure 1C). The MTRIPs bound to the hRSV gRNA and were assembled into cell-associated virions on the cell surface (Figure 1D). Virus was harvested from cells by scraping, aliquoting, and storage at −80 °C. After thawing an aliquot, virus was centrifuged through centrifugal membrane filters to remove cell debris and isolate filamentous virions, as well as spherical-like particles.[23]

In order to validate that MTRIP labeling did not significantly affect the virus, we monitored viral mRNA replication and protein expression during the first cycle of infection. We performed qRT-PCR for nascent hRSV phosphoprotein (P), polymerase (L), and major glycoprotein (G) mRNA at three time points postinfection (6, 12, and 24 h postinfection) and showed that there were no statistically significant changes in the transcript quantities generated by the MTRIP-labeled virus compared to unlabeled, wild-type virus at any of the time points examined (Figure 2A). We also performed Western blotting for the P and G proteins at 12 and 24 h postinfection to confirm that infection with the labeled virus expressed similar amounts of protein (Figure 2B). Blotting for the P protein produced a single band at the expected molecular weight for infections with labeled and unlabeled viruses. Blotting for the G protein produced multiple bands for the fully glycosylated and partially glycosylated versions of the protein for infections with labeled and unlabeled viruses.[24] We further quantified the amounts of protein using densitometry and found that at the time points examined there were no statistically significant changes in the amount of either P or G between the labeled and unlabeled infections (Figure 2C). We also spot-checked the total amount of protein produced at the 12 h postinfection time point by ELISA, using a polyclonal antibody against the whole virus (Figure 2D). No significant differences in the amounts of protein were

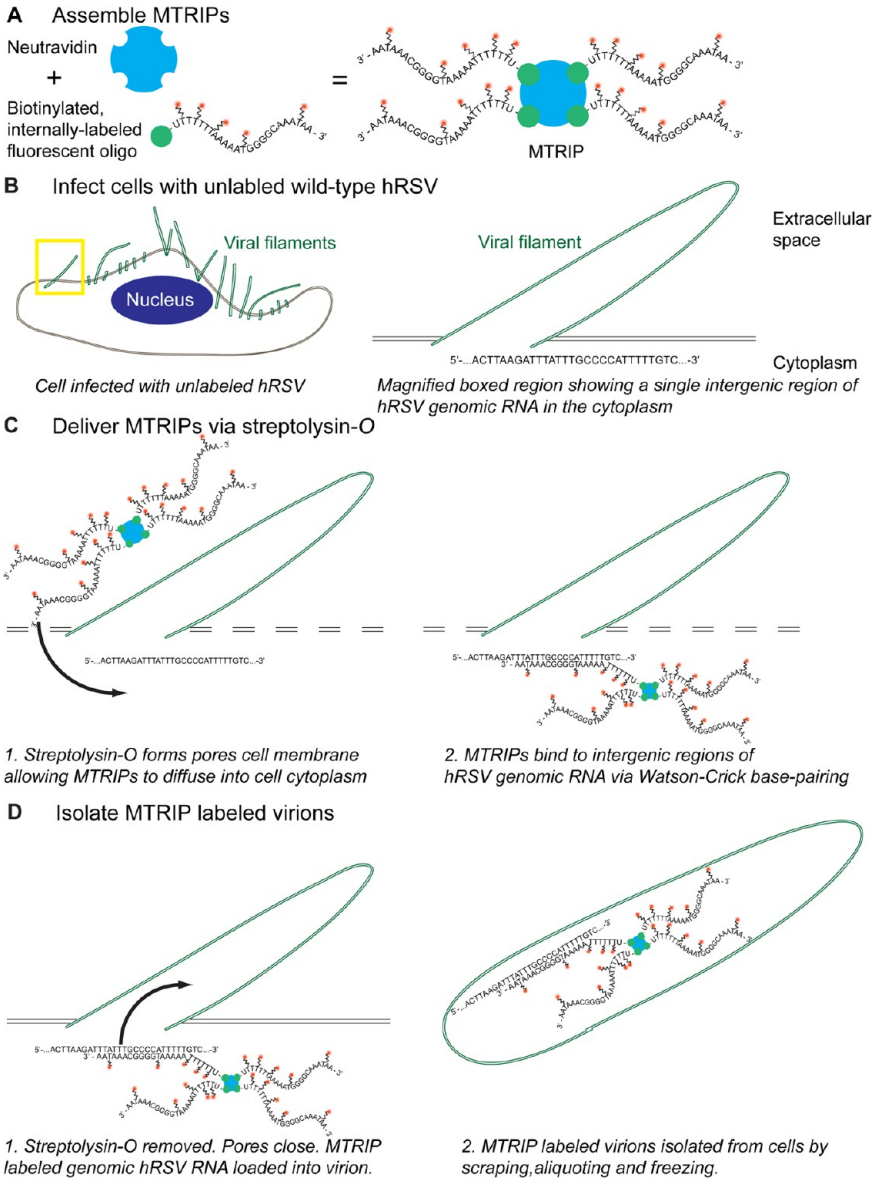

Figure 1. Illustration of MTRIP delivery and virus isolation methodology. (A) The MTRIP design consists of 2′-*O*-methyl RNA/DNA oligonucleotides that are internally labeled with fluorophores (red dots with carbon linkers on deoxythymidine nucleotides) and biotinylated on the 5′ end (green dot). These oligonucleotides are tetramerized by mixing them with neutravidin (blue circle). The actual probe sequence is shown. (B) HEp-2 cells were infected with hRSV for 96 h before MTRIP probe delivery. A depiction of a cell is shown on the left, and a viral filament protruding out of the cell membrane is shown on the right. A single intergenic sequence of the hRSV genome is shown just below the filament (the ellipsis on either end of the sequence represents the additional 15kb of the hRSV genome). (C) During probe delivery, streptolysin-O is used to permeablize the cell membrane (step 1), allowing MTRIP probes to diffuse into the cell cytoplasm and bind to the intergenic sites of the hRSV genome *via* Watson−Crick base-pairing (step 2). (D) Streptolysin-O is removed, allowing the pores in the cell membrane to reseal and the hRSV genome/MTRIP complex to be loaded into both spherical and filamentous virion (step 1). The labeled virions are detached from the cell by scraping and can be aliquoted and frozen for further experiments (step 2).

detected using this method either. Finally, we checked the virus titer later in the infection (96 h postinfection) to ensure that labeling did not affect the long-term kinetics of virus growth (Figure 2E). Both unlabeled and labeled viruses reached titers on the order of 10^6 pfu/mL, the maximum achievable titer without using high-density culture systems, and were not statistically different. These results show that MTRIP labeling does not significantly affect the hRSV replication cycle.

Futhermore, we examined the virus *via* transmission electron microscopy (TEM) to ensure that the labeling procedure did not affect virion morphology. We imaged cells infected with unlabeled virus, cells infected with unlabeled virus that had MTRIP probes delivered at 24 h postinfection, and cells that had been infected with labeled virus using thin section TEM (Figure 2F). In all three cases, infected cells generated filamentous and spherical virions, with characteristic electron dense envelopes and glycoprotein "spikes"

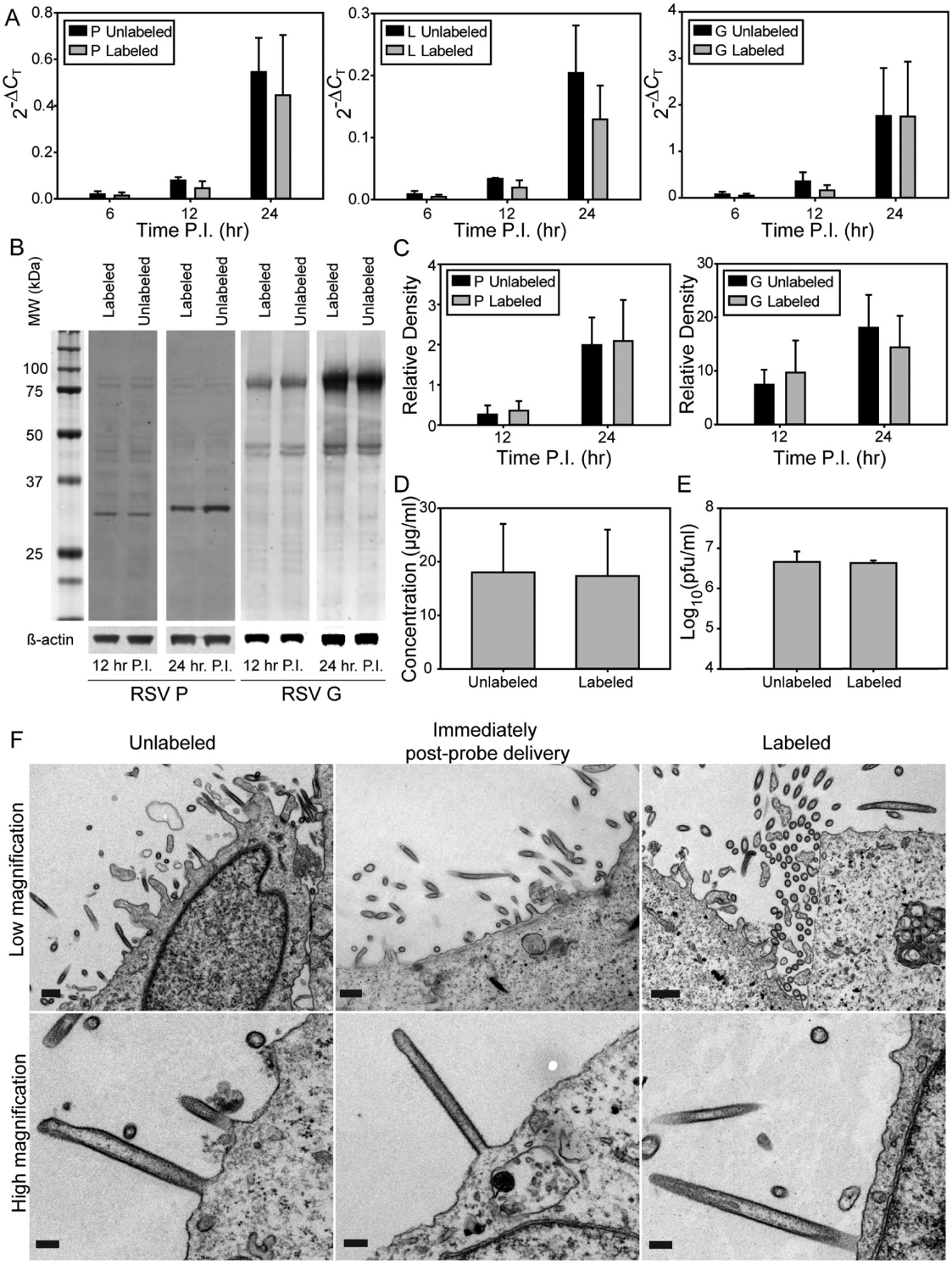

Figure 2. Validation of efficient virus replication and virus morphology of MTRIP-labeled virions. (A) Cycle threshold comparisons from qRT-PCR to detect nascent hRSV P, L, and G transcripts generated from infections of HEp-2 cells using labeled or unlabeled hRSV (multiplicity of infection (MOI) 0.1 at 6, 12, and 24 h postinfection). There were no statistically significant differences at any time point for any gene (*t* test, $n = 3$, $p > 0.05$). (B) Representative Western blots for hRSV P and hRSV G from cells infected with labeled or unlabeled virus (MOI 0.1 at 12 and 24 h postinfection) with representative molecular weight marker and β-actin loading control. (C) Replicate Western blots were further quantified by densitometry to compare signals from labeled and unlabeled virus relative to actin loading control. There were no statistically significant differences at any time point (*t* test, $n = 3$, $p > 0.05$). (D) Total hRSV protein ELISA from HEp-2 cells infected with labeled or unlabeled virus (MOI 0.1 at 12 h postinfection). There were no statistically significant differences (*t* test, $n = 3$, $p > 0.05$). (E) Plaque assay results for labeled and unlabeled virus grown in HEp-2 cells to a saturation point at 96 h postinfection. There were no statistically significant differences (*t* test, $n = 3$, $p > 0.05$). (F) Thin section TEM of Vero cells infected with unlabeled virus, unlabeled virus with MTRIP probes delivered immediately before fixation, or labeled virus (MOI 0.1 at 24 h postinfection). Low-magnification fields show the pleiomorphic nature of hRSV; high-magnification fields show single filamentous virions protruding from the cell surface. Scale bars 0.5 and 0.2 μm for low- and high-magnification images, respectively.

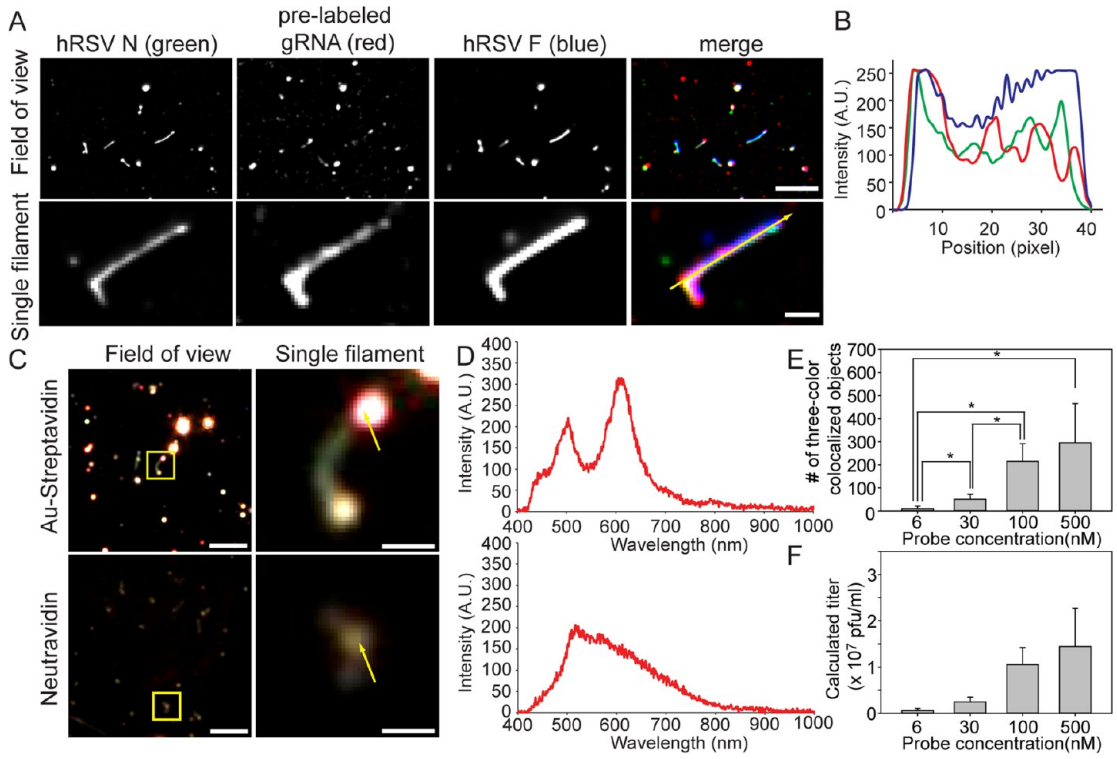

Figure 3. Characterization of MTRIP-labeled hRSV virions. (A) MTRIP-labeled virions were immobilized on a coverglass, and hRSV proteins N and F were detected *via* immunofluorescence. A representative field of view and a magnified filamentous virion are shown. The hRSV N (green), hRSV F (blue), and labeled gRNA (red) are shown individually as well as merged. (B) Profile plot of the fluorescence intensity along the length of the filament shown in part A. (C) Dark-field images of gold-streptavidin MTRIP-labeled hRSV and neutravidin MTRIP-labeled hRSV. Samples were silver enhanced prior to imaging. Field of view is shown on the left; boxed region indicates single filament featured in the magnified image to the right. (D) Spectra of light emitted from one pixel in the single-filament image (indicated by arrow) for Au-streptavidin-labeled virus (top) or neutravidin-labeled virus (bottom). (E) Effect of varying MTRIP probe concentration on the number of objects detected on the coverglass from infected cells containing hRSV N, hRSV F, and gRNA (above, Kruskal–Wallis one-way ANOVA, * indicates $p < 0.05$). (F) These numbers were used to calculate a theoretical estimate of viral titer. Single-plane, wide-field deconvolved images shown in part A. Scale bars are 5 and 1 μm, respectively. Single-plane, dark-field image is shown in part C. Error bars indicate standard deviation.

(low-magnification images). Close examination of filaments (high-magnification images) reveals filamentous virions 100 to 200 nm in diameter and over 1 μm in length in all three cases. From these images, it appears that MTRIP delivery and labeling does not affect virion morphology.

We then utilized fluorescence co-localization between the immunostained N and F proteins and the MTRIP-labeled gRNA to characterize the virions on coverslips (Figure 3A, Supporting Figure 1, Supporting Figure 2). We found that the distributions of the gRNA and N protein were discontinuous, whereas the F protein was distributed continuously (Figure 3A,B). To further verify that MTRIP probes were inside the virions, we replaced the neutravidin core of the MTRIP with a 5 nm gold nanoparticle/streptavidin conjugate. This change allowed us to image labeled virions on glass using dark-field microscopy, after reductive silver enhancement of the gold nanoparticles (Figure 3C). Since unbound probes were removed during centrifugation through membrane filters, the only MTRIPs in the sample were most likely inside of the virions. After isolating both neutravidin-MTRIP- and gold/streptavidin-MTRIP-labeled viruses and filtering to remove unbound probes, we detected a large peak in the gold/streptavidin-MTRIPs at around 620 nm, compared to the neutravidin-MTRIPs (Figure 3D). This peak was likely due to the increased plasmon scattering[25] of the silver-enhanced particles inside the virions.

Finally, the concentration of MTRIPs was titrated, and the number of particles containing gRNA and N and F was determined *via* blob co-localization[26] (Figure 3E). The number of three-color particles appeared to saturate upon delivery of 100 to 500 nM MTRIPs to infected cells. Unless otherwise noted, all subsequent virus labelings were carried out with a 100 nM probe. When the number of three-color particles for each concentration was used to calculate an approximate viral titer by extrapolating from number of particles on a 2D surface to a concentration of particles in a 3D volume (Figure 3F, Supporting Figure 3, Supporting Figure 4), the resulting numbers were within an order of magnitude of viral titers measured by plaque assay in Figure 2E, confirming that the labeled viral particles were likely infectious virions.

dSTORM Imaging of MTRIP-Labeled Filamentous Virions. To investigate how the distribution of gRNA compared to

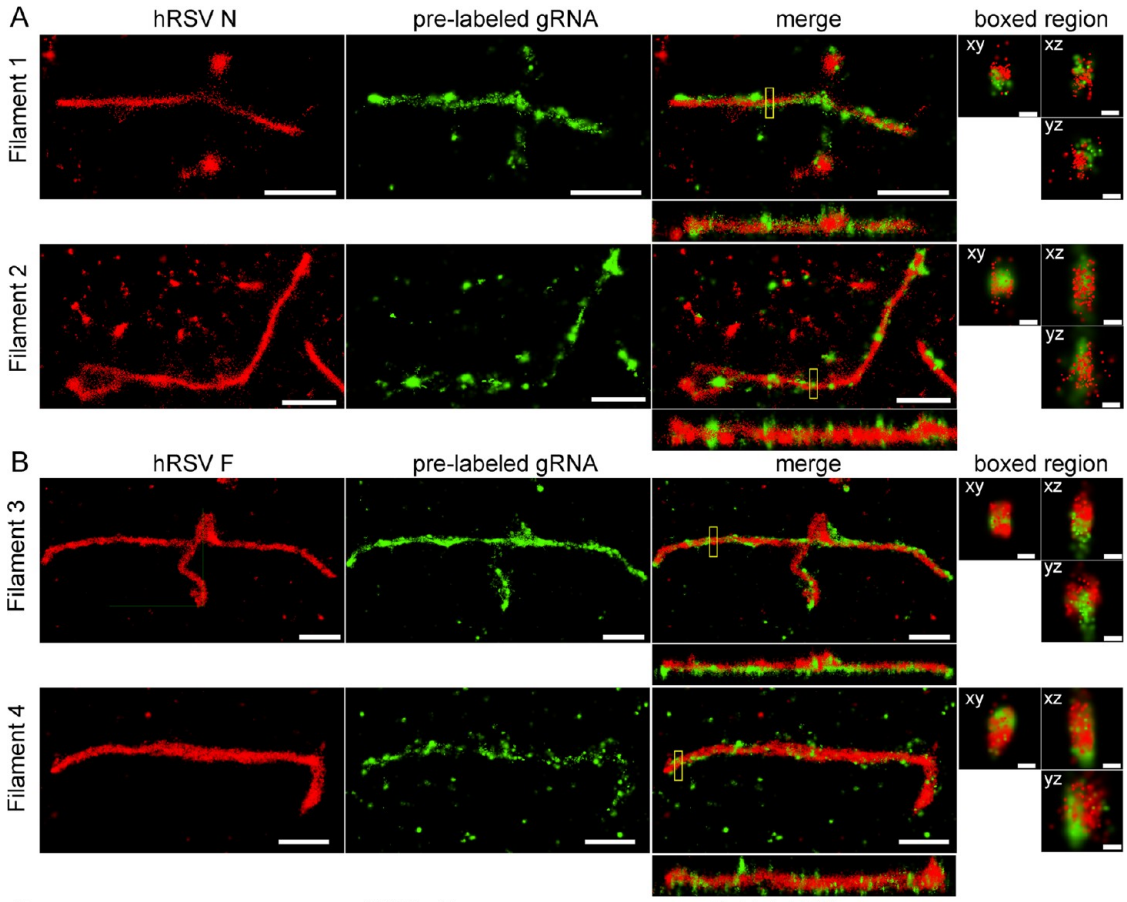

C

Image	hRSV N or F Lateral FWHM[a] (nm)	hRSV N or F Axial FWHM (nm)	Pre-labeled gRNA Lateral FWHM (nm)	Pre-labeled gRNA Axial FWHM (nm)
Filament 1	117	76	125	85
Filament 2	152	88	215	75
Filament 3	154	144	163	91
Filament 4	196	158	217	72

[a]FWHM – full width half maximum of point count

Figure 4. dSTORM images reveal spatial relationships between viral gRNA and viral proteins. (A) Two viral filaments showing the distribution of hRSV N (red), prelabeled gRNA (green), and merged image. A side view of the filament is shown below each merged image. The yellow boxed region represents a 100 nm long cross-section through the filament; the magnified *xy* (top), *xz* (side), and *yz* (front) projections of the cross-section are shown to the right of the merged image. (B) Two viral filaments showing the distribution of hRSV F (red), prelabeled gRNA (green), and merged image. Side view and boxed region are similar to those in part A. (C) Table describing the measured full width at half-maximum (fwhm) of the point count of the boxed regions. Lateral fwhm derived from *yz* projection of the cross-section shown in the boxed region. Axial fwhm derived from *xz* projection of the cross-section shown in the boxed region. Scale bars are 1 μm for whole filaments and 100 nm for the boxed region.

the distribution of viral proteins within filamentous virions, we used localization microscopy to image the labeled virions on coverslips. We found that the gRNA and N protein were distributed along the length of the filament, unevenly, for the first two example filaments shown (Figure 4A). However, the N protein did not co-localize exactly with the gRNA, suggesting that the N protein might not be bound to gRNA everywhere inside the virion. Upon examination of 100 nm cross sections through the filaments (boxed regions), we found that gRNA and N protein, in regions where they were both present, overlapped each other tightly. This finding was not the case for the F protein, which was distributed evenly along the length of the filaments and appeared in the cross section to surround, rather than overlap, the gRNA (Figure 4B). Note, the F protein was absent on the side of the filaments that was in contact with the glass. This finding likely was due to the antibody failing to access that side of the virion during immunostaining. These observations were quantified using the full width half-maximum (fwhm) of the point count for each channel for the cross sections shown (Figure 4C). While the axial fwhm did not differ significantly between measurements for the F and N proteins, the lateral fwhm for N was less than that of F and closer to the values for gRNA. These data clearly show that N and the MTRIP probes were in the interior of the virion, and the F protein was located further from the center of the virion.

MTRIP-Labeled hRSV Infections in Cell Culture. In addition to biochemical and plaque assays, we examined MTRIP-labeled virion replication in cell culture using

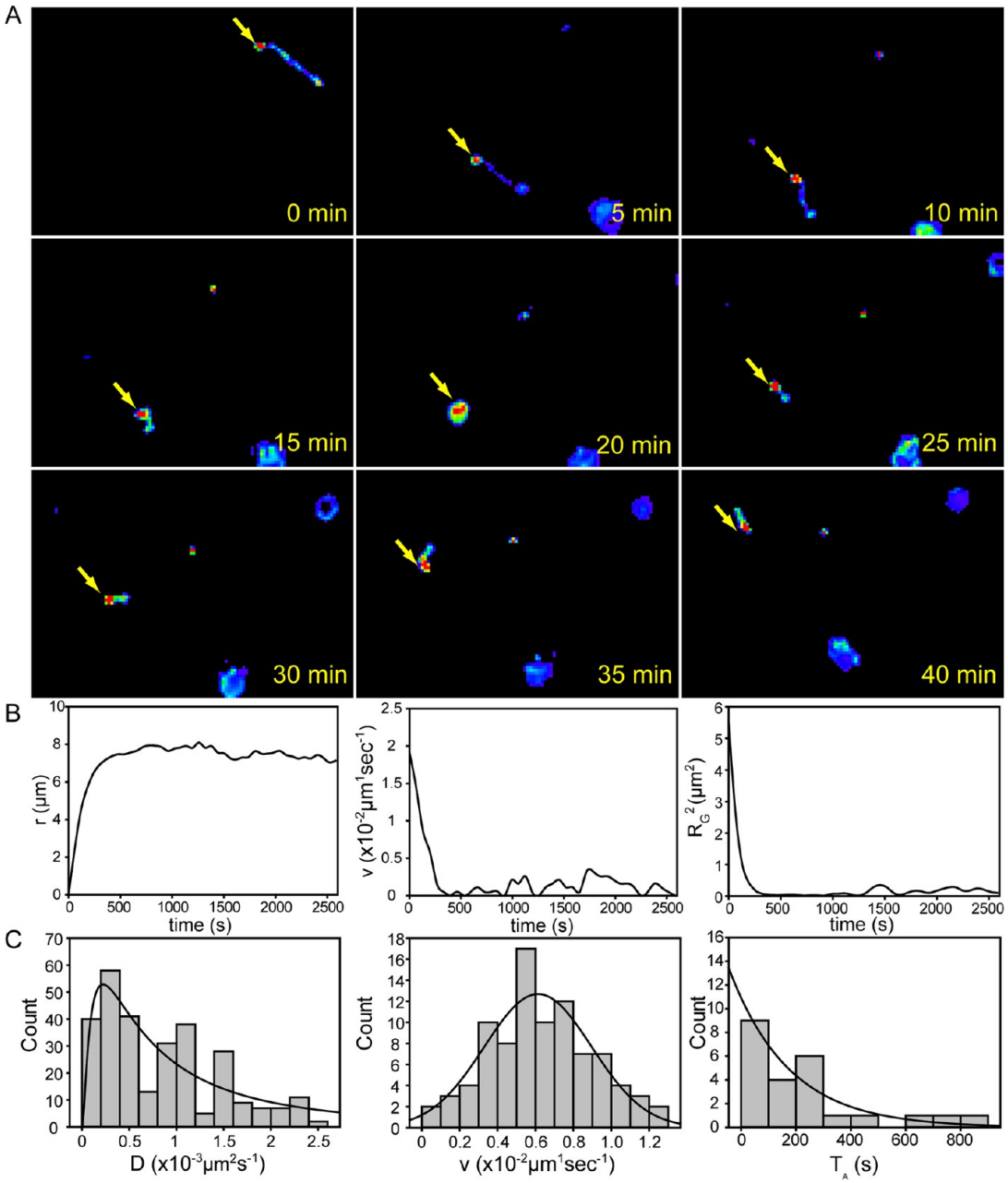

Figure 5. Single virion imaging reveals dynamic, largely diffusive behavior for MTRIP-labeled filamentous virions infecting cells. Cells were inoculated with MTRIP-labeled virions at 4 °C before live-cell imaging at 37 °C. (A) Frames from a typical live-cell video, acquired at 1 frame/min over the course of 40 min. Arrow indicates the end of the filamentous virion that was monitored *via* single-particle tracking. (B) Absolute displacement (from the position at $t = 0$ min), instantaneous velocity, and square of the radius of gyration over time for the virion shown in part A. (C) Histograms of the diffusion coefficient during passive states (left), instantaneous velocity for active states (center), and temporal duration of active states (right) for 15 individual filamentous virions over two different experiments. Black line indicates log-normal fit, Gaussian fit, and exponential decay fit, respectively. Single-plane, wide-field deconvolved images are shown.

fluorescence microscopy. After inoculating cells with MTRIP-labeled hRSV, we delivered MTRIPs with a different fluorophore and fixed the cells at subsequent time points (Supporting Figure 5). Fluorescence from the prelabeled gRNA was observed even at 48 h post-infection and remained co-localized with newly made gRNA and N protein. Infections with MTRIP-labeled virions produced filaments and inclusion bodies similar to infections with unlabeled virions.

Next, we compared MTRIP-labeled virion entry to a traditional GFP-based viral fusion assay, which uses citric acid to remove unbound virions from the surface of cells. A recombinant strain of RSV A2 expressing a GFP reporter gene in place of the hRSV small hydrophobic (SH) protein gene, rgRSV-GFP,[18] was labeled with MTRIPs using the same protocol as the conventional A2 strain. This MTRIP-labeled rgRSV-GFP was used to inoculate cells for different time durations

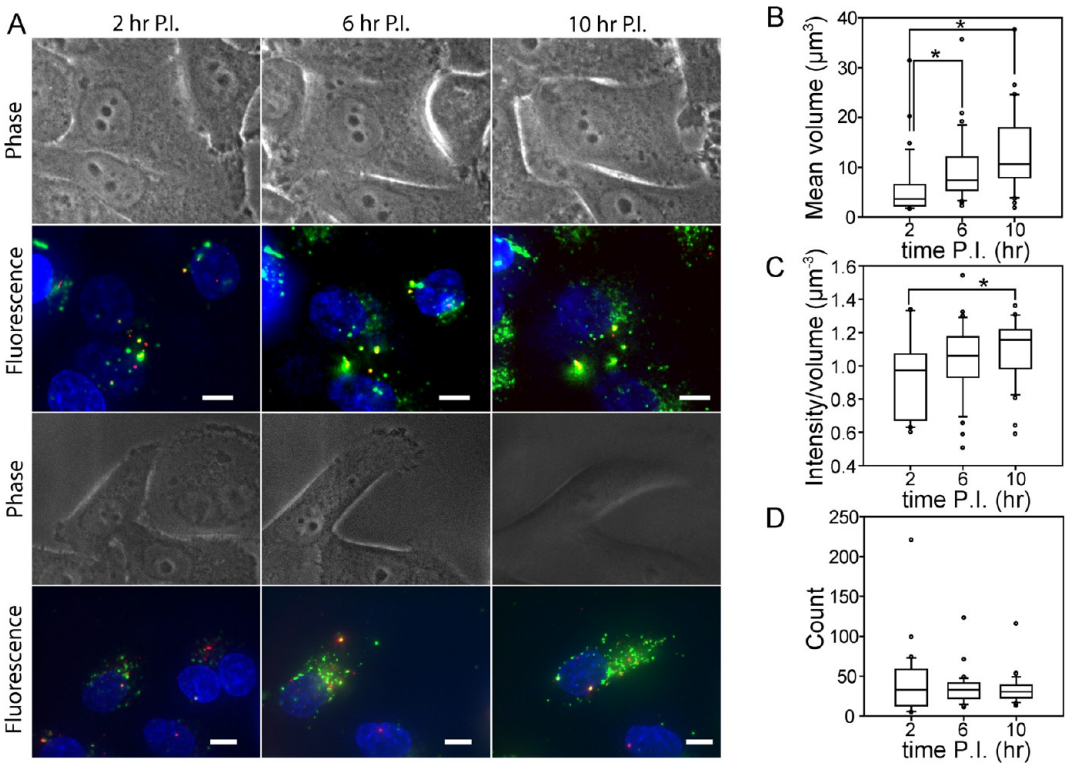

Figure 6. MTRIP-labeled hRSV virions can be used to follow the same cell over the course of an infection. HEp-2 cells were plated onto a patterned fibronectin substrate and infected with MTRIP-labeled hRSV. (A) Phase and fluorescence images for two different cells over an eight-hour period with prelabeled gRNA (red), newly produced gRNA (green), and cell nuclei (blue). (B) Mean fluorescence volume per puncta of the newly produced gRNA over the three time points. (C) Fluorescence intensity per volume of the newly produced gRNA over the three time points. (D) Number of newly produced gRNA puncta per cell over the three time points. One-way repeated measures ANOVA with Tukey test multiple comparison procedure; * indicates $p < 0.05$.

before unbound virions were inactivated with citric acid. Cells were imaged immediately after the citric acid wash, in order to count the number of labeled gRNAs inside cells, as well as 24 hours later to count the number of GFP-positive infected cells (Supporting Figure 6). The number of labeled gRNAs inside cells increased with time after inoculation, as did the number of GFP-positive cells. This finding suggests that the number of gRNAs, determined immediately after viral contact with the cells, could be used as a rapid indicator of virion fusion, as opposed to waiting up to 24 hours for GFP expression in the conventional assay.

In live cells, MTRIP labeling of virions was used to assist in the visualization of the dynamic nature of a filamentous virion infecting a single cell. MTRIP-labeled virions were adsorbed to a cell monolayer at 4 °C and then imaged at 37 °C over the course of 40 min (Figure 5A, Supporting Movie 1). The resulting videos showed a dynamic process, including periods of motion, rest, and changes in morphology of the filament. In an attempt to quantify whether this motion was the result of active or passive transport, we examined the absolute displacement, relative to the start coordinates, as well as the velocity and radius of gyration of a point on the filament (Figure 5B).[27−29] We segmented the tracks over a rolling window of 4 min. This analysis showed that after an initial temperature-dependent transient motion (which we defined as the first 5 min of recording), filaments displayed small peaks in velocity accompanied by periods of little motion, leading to small changes in the absolute displacement. However, when the radius of gyration extent parameter was considered, these peaks were smaller and similar to the baseline values. Results from Monte Carlo simulations indicated that a threshold of $R_G^2 = 0.3\ \mu m^2$ was sufficient to discriminate between periods of active and diffusive motion for a model virion (Supporting Figure 7). On this basis, trajectory segments were classified as either passive or active, as opposed to using the velocity directly. Using this threshold, we generated histograms of diffusion coefficients (for passive states) or velocities (for active states), as well as the time duration of active states for 15 virion tracks (Figure 4C). For passive states, a log-normal fit obtained a median diffusion coefficient of $8.8 \times 10^{-4}\ \mu m^2\ s^{-1}$. For active states, a Gaussian fit obtained a mean velocity of $6.1 \times 10^{-3}\ \mu m\ s^{-1}$. For the temporal duration of active states, the data were fitted to an exponential decay with a median time of 6.3×10^{-2} s. These measurements indicated that the motion exhibited by a virion undergoing fusion was largely diffusive, with short, nonlinear durations of active transport interspersed during the course of observation.

We confirmed that the motion and shape changes of the filaments were most likely due to fusion and not endocytosis by immunostaining for markers of early (EEA1) or late (CD63) endosomes and lysosomes (LAMP1). Labeled gRNA did not co-localize with any of these markers (Supporting Figure 8). We also recorded live-cell videos of filamentous virion dynamics in cells transduced with a baculovirus adapted to mammalian cell culture expressing Rab5-GFP, showing that Rab5 did not accumulate around a filament as it underwent fusion (Supporting Figure 8, Supporting Movie 2). Taken together, these results indicate that the changes in morphology and motion of a filament during fusion to cells were not due to endocytosis, but rather due to the viral fusion process with the cell membrane.

It should be noted that along with imaging hRSV viral filament RNA entry we did attempt to combine this strategy with membrane labeling using the carbocyanine lipophilic dye DiO, which is typically used in this sort of assay. Unlike more structured viruses, hRSV filamentous virions did not label efficiently with DiO (Supporting Figure 9). Cells decorated with high numbers of filaments were largely unlabeled, while neighboring cells, lacking filaments, were labeled efficiently, as were noninfected cells (Supporting Figure 9). Only the spherical-like particles were labeled with DiO, precluding its use in interrogating filamentous virion entry.

Finally, we used MTRIP-labeled virions to track the same set of live cells as they progressed through an hRSV infection. Using cells plated on a fibronectin-patterned 35 mm coverslip-bottomed dish, we watched HEp-2 cells inoculated with hRSV for eight hours, delivering MTRIP probes, labeled with a spectrally distinct fluorophore from those labeling the virion, every four hours to monitor new gRNA production (Figure 6A). The combination of cell patterning and MTRIP-labeling allowed the same cell to be relocated and imaged over multiple time points. By delivering MTRIPs with a spectrally distinct fluorophore at varying time points, we were able to quantify changes in the volume, intensity, and number of nascent gRNA puncta on a per-cell basis (Figure 6B,C,D, respectively). It is clear that while the number of gRNA puncta did not change significantly, the sizes of the puncta increased dramatically, accompanied by a small, but significant increase in the normalized intensity. This finding suggested that once hRSV gRNA entered the cell, it was confined to certain sites of replication and did not diffuse readily throughout the cytoplasm.

Our approach provides a method to analyze the distribution of RNA and multiple viral proteins within virions simultaneously, using both conventional and localization microscopy. While the imaging analysis of virus on glass has been attempted before using either membrane labeling[3] or fluorescence *in situ* hybridization (FISH),[30] these methods detected the viral envelope (membrane labeling) or an internal RNA (FISH), not both at the same time. FISH requires fixation, membrane permeabilization, and the use of formamide, which can inhibit antibody binding for identification of proteins. Our labeling method combined with dSTORM enables the analysis of RNA/protein distributions in virions with fluorescence at a resolution (20 nm laterally) smaller than the width of a virion (200 nm width of filament).[20,23] Given the fact that the gRNA was distributed throughout the length of the filament and that gRNA granules were quite large (~80 nm laterally), it is likely that there is more than one copy of the hRSV genome within large filamentous virions, especially since the helical gRNA and N complex is thought to be only 10 nm wide.[31] This feature is not the case for other filamentous virions such as the filovirus Ebola, which makes filamentous virions that contain only one genome[32] and is part of the same *Mononegavirales* order as hRSV. However, the correlation between incorporation of multiple copies of RNA viral genomes and viral replication efficiency has yet to be established. Future work could include using localization microscopy to investigate the distribution of other viral proteins such as the matrix (M) protein and cellular proteins (such as F-actin) within the filament. This approach might help better define principal mechanistic determinants of filament formation, which are still unclear.[22,33−37]

We also analyzed the dynamics of a filamentous virion undergoing fusion for the first time. The only other filamentous virion to have been labeled and imaged in a live cell is Ebola,[10,16] and that analysis was limited to the co-localization of endocytic markers with GFP-viral fusion proteins (as Ebola traffics through the macropinosome). The passive motion of filaments during fusion merits further investigation. The velocity in the active states was not as high as those reported for virus surfing along filopodia,[1] and these states constituted a minority of the observed motion. Rather, the largely passive motion we observed might be due to virus attachment to cell surface lectin-like molecules by the highly glycosylated hRSV G surface glycoprotein followed by diffusion along the membrane and binding of the particles to a *bona fide* cell surface receptor, such as nucleolin,[38] which triggers fusion. An alternative hypothesis might be that the virus diffuses after first being recruited to a lipid raft.[12,39] To date, the study of paramyxovirus fusion proteins has been focused on the ultrastructure of the protein in different conformational states;[40] the ability to observe fusion dynamically could enhance these studies.

The ability to watch gRNA replication in a single cell allowed several important biological observations with implications for both hRSV and other viruses. For hRSV, we observed that, in general, the overall number of granules increased slowly over time, but that the volume increased at a higher rate, suggesting that these granules were replication complexes. These complexes have not

been defined previously, only assumed. The data also showed the inherent heterogeneity of cell features during hRSV infections, which previous imaging studies have revealed, but had yet to be quantified. For viral infections, this approach has the means to ask and answer fundamental questions regarding the sources of heterogeneity of viral infections, because the initial conditions of each cellular infection can be defined, and the infection characterized within the same cells. This method clearly will assist in the quantification and development of mechanistic models of cell-to-cell variation during viral infections.

The MTRIP probe design has several distinct advantages over other virus-labeling methods. Since each MTRIP is labeled with 8−12 fluorophores, fewer probes are required to produce a single molecule sensitive fluorescence intensity than other methods such as single fluorophore FISH,[41] increasing sensitivity. Organic fluorophores are also more resistant to photobleaching than fluorescent proteins. While quantum dots have also been used for virus labeling,[42] their size and toxic effects limit their ability to observe the viral gRNA over long periods of time. For high frame rate imaging of viral dynamics, the blinking of the fluorescence intensity of quantum dots[43] might introduce artifacts in single-particle tracking and deconvolution algorithms. MTRIPs do not blink under normal buffer conditions and wide-field illumination, avoiding this problem. By designing different biotinylated oligonucleotides to bind to different virion sequences, they can be easily adapted to target to different regions on the gRNA, allowing for the possibility of increasing fluorescence intensity in particle tracking experiments and for increased localization accuracy in super-resolution microscopy. Lastly, the addition of gold nanoparticles to the neutravidin core of the MTRIP allowed for dark-field imaging *via* silver enhancement, making labeled RNA TEM imaging possible. Most importantly, the MTRIP labeling method does not affect the first cycle of virus replication, the titer during amplification, or the virus morphology.

CONCLUSION

In summary, MTRIP labeling of viral RNA has the potential to become a general methodology for the labeling and study of many different RNA viruses. Assuming unique target sequences can be found within a given virus's genome, MTRIP probes could be designed to bind to it, making our technique broadly applicable to most virus studies. The approach could also be combined with conventional membrane-labeling techniques and fluorescent fusion protein technology to yield multicolored virions suitable for live-cell observation of virion infection over the entire replication cycle.

METHODS

MTRIPs. MTRIP probe design is described in more detail elsewhere.[17] Briefly, 2′-*O*-methyl RNA/DNA chimeric nucleic acid ligands (targeting the intergenic-gene start sequences of the hRSV A2 genome) containing a 5′-biotin modification (Biosearch Technologies) were labeled with either Cy3B NHS ester (GE Healthcare) or DyLight 650 NHS esters (Pierce). Unbound dye was removed *via* centrifugation in a 3 kDa filter (Millipore) and stored at −20 °C until further use.

To assemble probes, labeled oligonucleotides were mixed with neutravidin (Pierce) in a 5:1 molar ratio and allowed to react at room temperature for 1 h. Unbound oligonucleotides were removed by centrifugation in a 30 kDa filter (Millipore).

Cell Culture. HEp-2 human epithelial cells (American Tissue Culture Collection CCL-23) and Vero green monkey kidney cells (CCL-81) were maintained in DMEM (Lonza) supplemented with 10% fetal bovine serum (Hyclone) and 100 U mL^{-1} penicillin and 100 mg mL^{-1} streptomycin (Invitrogen). Cells were plated on No. 1.5 coverslips (Electron Microscopy Sciences) or 35 mm coverslip-bottomed dishes (In Vitro Scientific) one day prior to infection or imaging.

Probe Delivery. Cells were washed in Dulbecco's phosphate-buffered saline (DPBS) without Ca^{2+} and Mg^{2+} (Lonza) and subsequently incubated with OptiMEM I (Invitrogen) containing 30 nM MTRIP probes and 0.2 U mL^{-1} activated streptolysin O (Sigma) for 10 min at 37 °C. Afterward, the OptiMEM was replaced with complete growth media for 15 min at 37 °C before fixation, imaging, or harvesting virus.

Virus Propagation. hRSV strain A2 (American Tissue Culture Collection VR-1544) or rgRSV-GFP (a gift from Martin L. Moore's lab, Emory Univ.) was propagated in low-passage HEp-2 cells when the cells were >80% confluent. The medium was removed from the cells, the cells were washed with DPBS (without Ca^{2+} and Mg^{2+}), and virus was added at a multiplicity of infection (MOI) of 0.1 for 1 h before adding fresh medium to the inoculum. Cell-associated virus was harvested by scraping when the cells displayed a high degree of cytopathic effects (approximately 90%, or around 96 h postinfection), vortexed briefly, aliquoted, and stored at −80 °C.

For MTRIP-labeled virus, MTRIP probes were delivered to cells according to the Probe Delivery section before the cells were scraped.

Plaque Assay. In order to quantify the titer of unlabeled and labeled hRSV, aliquots of frozen virus were thawed, and equal volumes of labeled and unlabeled virus (from Virus Propagation section) were serially diluted from 10^{-2} to 10^{-6} and used to inoculate 24-well plates of 100% confluent Vero cells in quadruplicate. Inoculant was allowed to incubate for 1 h before cells were covered with 1 mL per well of 1.2% microcrystalline methylcellulose (Avicel, FMC Biopolymer) in growth media, similar to Matrosovich *et al.*[44] The cells were incubated with overlay for 6 days postinfection, when visible, uniform plaques ∼3 mm in diameter had formed. The cells were fixed with 4% paraformaldehyde, blocked with 5% BSA, and stained using a primary antibody and secondary HRP conjugated antibody (listed in Antibodies section) for incubation times similar to the immunostaining protocol below. A peroxidase substrate was added after washing (TrueBlue, KPL) and allowed to develop for 10 min before washing again. Dilutions with countable numbers of plaques (between 5 and 50) had their plaques counted, averaged over the four replicate wells, and multiplied by the dilution factor to calculate the titer in pfu/mL. This assay was done for three aliquots per batch of virus grown, and the average titer of the three aliquots was used to normalize the number of input virus between unlabeled and labeled virus for all subsequent experiments with that virus batch.

qRT-PCR. HEp-2 cells were plated in six-well plates the day before infection at >80% confluence. Cells were infected with unlabeled or labeled virus at an MOI of 0.1 for 6, 12, or 24 h postinfection. Total RNA was extracted using an RNeasy kit (Qiagen)

following the manufacturer's protocol. After quantification, mRNA was isolated from total RNA using an Oligotex kit (Qiagen) following the manufacturer's protocol. cDNA synthesis was performed using 70.4 ng of mRNA and a First Strand Reaction kit (SA Biosciences) according to the manufacturer's protocol. qRT-PCR was performed in triplicate using the Universal MasterMix (Applied Biosystems), Taqman probe/primer sets described in Thornburg *et al.*,[45] and a Step-One Plus real-time thermocycler (Applied Biosystems). Human GAPDH probe/primers (Applied Biosystems) were used as a loading control. Cycle threshold detection was performed using the Applied Biosystems software. Infections and extractions were repeated three times.

Western Blotting. HEp-2 cells were plated in six-well plates the day before infection at >80% confluence. Cells were infected with unlabeled or labeled hRSV at an MOI of 0.1 for 12 or 24 h postinfection. Cells were lysed by adding RIPA buffer (Pierce) spiked with 50× Complete Protease Inhibitor (Roche), scraping, and clarifying by centrifugation. Protein concentration was quantified using a BCA assay (Pierce) following the manufacturer's protocol. Lysates were stored at −80 °C until use.

For SDS-PAGE gel, 12 μg of lysates was mixed with a 4× SDS loading buffer (LI-COR Biosciences), boiled for 10 min at 70 °C, chilled on ice, and loaded into wells of a 10% Bis-Tris precast gel (Invitrogen) along with a molecular weight marker (LI-COR). Gel was run in an XCell Surelock Mini Cell system (Invitrogen) in 1× MOPS running buffer (Invitrogen) at 200 V constant for 50 min. Protein was transferred to 0.45 μm pore nitrocellulose membranes (Invitrogen) using an XCell II Blot module (Invitrogen) running at 30 V constant for 1 h in 1× western transfer buffer (Invitrogen).

Blots were stained using a Snap i.d. blot holder (Millipore). First, nonspecific binding was blocked using blocking solution (LI-COR). Vacuum was immediately turned on for 20 s to remove solution. Next, the primary antibody against the protein (along with a β-actin antibody) was added and allowed to incubate for 10 min. Vacuum was turned on and blots were washed three times with 1× PBS containing 0.1% Tween-20. Finally, the secondary antibodies was added and allowed to incubate for 10 min. Blots were washed three times with PBS containing Tween-20 and then imaged using an Odyssey IR imager (LI-COR). Exposure times and gain settings were kept fixed for each protein, and only linear contrast enhancement was performed for the final representative image. Each isolation was performed three times, and all blots were quantified by densitometry using the Image Studio software package (LI-COR). Total signals in the 700 nm channel were recorded using a rectangular ROI that covered ~1/3 the lane width and the entire lane length.[46] Background was subtracted using a median filter to find the actual protein signal. This procedure was repeated for β-actin in the 800 nm channel, and the protein signal was divided by the actin signal for each lane (replicate extraction) to yield the relative density.

Enzyme-Linked Immunosorbent Assay. A total hRSV protein ELISA kit (Bioo Scientific) was used according to the manufacturer's protocol using 100 μg of protein per well. Each sample was assayed in duplicate, and three samples (from three different infections and extractions) were done for each condition (labeled or unlabeled).

Thin Section Transmission Electron Microscopy. Vero cells were plated in a six-well plate at >80% confluence and were infected with unlabeled or labeled virus (MOI 0.1). At 24 h postinfection, probes were delivered to one set of cells infected with unlabeled virus (for "immediately post probe delivery" condition), and all cells were fixed overnight at 4 °C with 2.5% glutaraldehyde in 0.1 M cacodylate buffer (pH 7.4, Electron Microscopy Sciences). Cells were then washed and postfixed in 1% osmium tetroxide with 1.5% potassium ferrocyanide in the same buffer for one hour. The samples were subsequently rinsed with 2 or 3 exchanges of deionized water, dehydrated through an ethanol series ending with three exchanges of 100% absolute ethanol, and embedded in Eponate 12 resin (Ted Pella) by placing resin-infiltrated cells in a 60 °C oven for 2 days.

Upon resin polymerization, hardened resin blocks with monolayer cells on the bottom surface were removed from the culture plate, sawed into smaller pieces, and thin-sectioned perpendicular to the cell surface at 70 nm. Sections were then picked up with 200 mesh Formvar-coated copper grids, stained with 5% aqueous uranyl acetate and 2% lead citrate, and viewed on a JEOL JEM_1400 transmission electron microscope equipped with a Gatan US1000, 2k × 2k CCD camera.

Virus Infection. In all imaging experiments (not virus propagation), unlabeled or labeled virus used for infecting cells was first centrifuged through 5 and 0.45 μm filters (Millipore) at 5000*g* and 4 °C for 4 and 1 min, respectively, to isolate single filaments. This filtration is important for imaging experiments, because it removes the dead cell debris from the cell-associated hRSV. The cell debris complicates the imaging of single filamentous virions on glass or in cells. However, this centrifugal filtration leads to a loss of infectivity, regardless of whether or not the virus is labeled, because some virus sticks to the filter membrane. Hence, to compensate for this loss in virus, the initial volume of virus filtered was calculated using the titer for that batch, desired MOI for that experimental design, and a scalar factor characteristic of the filters. For example, for an experiment with a desired MOI of 1 involving 100 000 cells per well, a virus batch with a titer of 1×10^6 pfu/mL, and a filter correction factor of 2 (about 50% of viruses are lost in the filter), the initial volume of virus needed (before filtration) would be

$$100\,000\ \frac{\text{cells}}{\text{well}} \times 0.1 \frac{\text{virions}}{\text{cell}} = 10\,000 \text{ virions postfiltration}$$

$$10\,000 \text{ virions} \times 2 = 20\,000 \text{ virions prefiltration}$$

$$20\,000 \text{ virions} \times \left(1 \times 10^6 \frac{\text{pfu}}{\text{mL}}\right)^{-1} = 0.020 \text{ mL virus needed prefiltration}$$

The stated MOI for both the labeled and unlabeled viruses (seen in most figure captions) accurately reflects this adjustment in the volume.

Cells were chilled on ice at 4 °C to prevent endocytosis and synchronize virion fusion. Cells were then washed with chilled DPBS (without Ca^{2+} and Mg^{2+}), and virus in chilled growth medium was added to the cells and allowed to adsorb for 30 min on ice at 4 °C. Afterward, cells were moved to an incubator at 37 °C, and the virus was allowed to fuse for 2 h before being removed and replaced with complete growth media, except for the filament dynamics experiments, which were imaged immediately after adsorption of virus and after 5 min in the live-cell environment to bring them up to 37 °C.

Immunostaining. Cells or virus on coverslips were fixed in 4% paraformaldehyde (Electron Microscopy Sciences) in PBS for 10 min at room temperature before permeabilization with 0.2% Triton X-100 (Sigma) for 5 min at room temperature. This step was followed by blocking with 5% bovine serum albumin for 30 min at 37 °C, washing with PBS, primary antibody incubation for 30 min at 37 °C, washing with PBS, secondary antibody incubation for 30 min at 37 °C, and a final washing with PBS. Multiple antibody labeling was done simultaneously after checking for cross-reactivity. Cells then were stained with DAPI, and all samples were mounted with Prolong Gold (Invitrogen).

For virus on glass, before fixation, virus was centrifuged through the filters used for infecting cells. This size fraction then was spun down onto poly-L-lysine (Sigma)-coated coverslips *via* centrifugation at 3007*g* and 4 °C for 30 min. Virus then was fixed and immunostained using the above method.

Antibodies. For Western blot, the primary antibodies used were a mouse monoclonal anti-hRSV G (Abcam) and a mouse monoclonal anti-hRSV P (clone 3_5, a kind gift of Earling Norrby and Ewa Bjorling). Secondary antibodies used were donkey anti-mouse DyLight 680 (Pierce) and donkey anti-rabbit IRDye 800 (LI-COR).

For plaque assay, the primary antibody used was a goat polyclonal anti-hRSV (Abcam). The secondary antibody was a donkey anti-goat HRP (Jackson Immunoresearch).

For imaging, primary antibodies used were mouse anti-hRSV N (Abcam), human anti-hRSV F (MedImmune), mouse anti-EEA1 (BD Biosciences), mouse anti-CD63, and mouse anti-LAMP1 (both from Developmental Studies Hybridoma Bank).

Secondary antibodies used were donkey anti-mouse Alexa Fluor 488 (Invitrogen), donkey anti-human DyLight 650, and donkey anti-human Alexa Fluor 647 (Jackson Immunoresearch).

Fixed- and Live-Cell Imaging. Images for fixed-cell pulse-chase experiments (Figure 2) were taken on an LSM 710 laser scanning confocal microscope (Zeiss) with a 63×, NA 1.4 plan-apochromat objective. hRSV N and prelabeled gRNA were taken on separate tracks to minimize bleed through; DAPI and postinoculation gRNA were taken on the same track. Lasers used for DAPI, hRSV N, prelabeled gRNA (Cy3B), and postinoculation gRNA (DyLight 650) were 405, 488, 555, and 635 nm, respectively. Z stacks were taken in increments of 0.4 μm, with pinhole set to 1 Airy disk.

All other images were taken on an Axiovert 200 M inverted microscope (Zeiss) with a 63×, NA 1.4 plan-apochromat objective and ORCA-ER AG camera (Hamamatsu). The 89000 Sedat Quad-ET filter set (Chroma) was used. Z stacks were taken in increments of 0.2 μm. Images were acquired using Volocity software (Perkin-Elmer).

Live-cell experiments were taken using cells in 35 mm coverslip bottom dishes with Leibovitz's CO_2 independent L-15 medium (Invitrogen) supplemented with 10% FBS medium. Dishes were kept warm during imaging using a Chamlide TC-L live-cell environment (Live Cell Instrument). Images were taken using a C9100-02 EMCCD camera (Hamamatsu).

Image Processing. All wide-field images were deconvolved using Volocity. All object finding and counting was conducted using Volocity and exported to Excel (Microsoft) or Sigma Plot (Systat) for graphing and statistical analysis. Exceptions include probe titration, for which the blob co-localization was computed by exporting TIFF images for each channel from Volocity and using the ImageJ plugin described in Fletcher *et al.*[26]

Live-cell videos taken with the EMCCD camera were denoised using the ND-Safir binary for Windows described by Boulanger *et al.*[47] using the default settings. Videos were exported from Volocity as TIFF files and assembled into stacks by time point using custom programs in MATLAB (MathWorks), and the ND-Safir binary was called repeatedly to process each time point. Videos were reassembled in Volocity for deconvolution.

Single-particle tracking of filaments was performed manually in Volocity. Manual track coordinates were exported *via* CSV file into MATLAB. Rolling window temporal analysis and Monte Carlo simulations were carried out using custom programs. Results were graphed and fitted using Sigma Plot.

Linear contrast enhancements were performed on images and videos for clarity. All calculations were performed on unenhanced, deconvolved data.

Dark-Field Imaging. Optical and hyperspectral images along with hyperspectral data were captured utilizing a research-grade optical microscope equipped with the CytoViva advanced dark-field illumination system dual-mode fluorescence module and integrated hyperspectral imaging system (CytoViva, Inc., Auburn, AL, USA). This integrated system builds hyperspectral image files by a "push broom" method, enabling the creation of a high signal-to-noise spectral image file. Subsequent image analysis delineates the reflectance spectral response of the sample elements in each nanoscale pixel of the image file.

dSTORM Imaging. Super-resolution images were recorded with a Vutara SR 200 (Vutara, Inc., Salt Lake City, UT, USA) commercial microscope based on the single-molecule localization biplane FPALM technology.[48,49]

Viral proteins and MTRIP probes were imaged using 647 and 561 nm excitation lasers, respectively, and 405 nm activation laser in a photoswitching buffer composed of 20 mM cysteamine and oxygen scavengers (glucose oxidase and catalase) in 50 mM Tris+10 mM buffer at pH 8.0. Images were recorded using a 60×, NA 1.2 water immersion objective (Olympus) and Evolve 512 EMCCD camera (Photometrics) with gain set at 50, frame rate at 50 Hz, and maximal powers of 647, 561, or 405 nm lasers set at 8, 8, or 0.05 kW cm^{-2}, respectively. Total number of frames acquired per channel ranged from 2000 to 4000 frames.

Data were analyzed by the Vutara SRX software (version 4.07). Single molecules were identified by their brightness frame by frame after removing the background. Identified particles were then localized in three dimensions by fitting the raw data in a customizable region of interest (typically 16 × 16 pixels) centered on each particle in each plane with a 3D model function that was obtained from recorded bead data sets. Fit results were stored as data lists for further analysis. The image resolution capable of experimentally being achieved is 20 nm laterally (*x* and *y*) and 50 nm axially (in *z*).

Fusion Assay. Inoculation of cells with MTRIP-labeled rgRSV-GFP occurred as described above. Virions were allowed to fuse for a designated time at 37 °C before being washed with a 40 mM sodium citrate solution containing 10 mM potassium chloride and 135 mM sodium chloride (Sigma) adjusted to pH 3.0. Cells were imaged immediately afterward in L-15 growth media and then allowed to sit in complete growth media for 24 h before being imaged again.

Transduction. Cells were transduced with a Rab5-GFP baculovirus adapted for mammalian cell culture, following the manufacturer's protocol (Invitrogen).

Live-Cell Virus Replication. Micropatterned substrates to control cell spread area and clustering were prepared by microcontact printing of fibronectin, as has been previously described.[50] Briefly, stamps made from PDMS (Sylgard 184 elastomer kit, Dow Corning) consisting of 100 × 100 μm squares were plasma cleaned and inked with 50 μg/mL human plasma-purified fibronectin. Stamps were dried under nitrogen gas, and protein was transferred onto acid-washed No. 1.5 coverglass or 35 mm coverslip-bottomed dishes. The substrates were then blocked with 10% heat-denatured bovine serum albumin to prevent nonspecific cell attachment. Cells were plated the day before infection, inoculated as described above, and had 30 nM DyLight 650 MTRIP probes delivered to them at 2 h postinfection and every 4 h thereafter. Cells were left in the Chamlide live-cell environment in L-15 medium supplemented with FBS to facilitate relocation of the same cells.

Conflict of Interest: The authors declare no competing financial interest.

Acknowledgment. This work was supported by NIH grant R01GM094198 (P.J.S.). We would like to acknowledge Andrew Shaw and the Microscopy and Biophotonics Core Facility of the Parker H. Petit Institute for Bioengineering and Bioscience at Georgia Tech for use of their confocal microscopes and real-time thermocycler. We would also like to acknowledge Dr. Natalie Thornburg and Dr. Jennifer Pickens at Vanderbilt for their help with primer/probe sets for the hRSV genome.

Supporting Information Available: Images of antibody staining controls, centrifugation controls, particle density controls, MTRIP probe titration, MTRIP-labeled hRSV infected cells at varying time points, MTRIP-labeled hRSV fusion assay, Monte Carlo simulations of active and passive transport, co-localization with endosomal compartments, and DiO labeling of hRSV are provided. Live-cell imaging movies of single-filament fusion and single-filament fusion in Rab5-GFP transduced cell also provided. This material is available free of charge *via* the Internet at http://pubs.acs.org.

REFERENCES AND NOTES

1. Lehmann, M. J.; Sherer, N. M.; Marks, C. B.; Pypaert, M.; Mothes, W. Actin- and Myosin-Driven Movement of Viruses along Filopodia Precedes Their Entry into Cells. *J. Cell Biol.* **2005**, *170*, 317–325.
2. Brandenburg, B.; Lee, L. Y.; Lakadamyali, M.; Rust, M. J.; Zhuang, X.; Hogle, J. M. Imaging Poliovirus Entry in Live Cells. *PLoS Biol* **2007**, *5*, e183.
3. Coller, K. E.; Berger, K. L.; Heaton, N. S.; Cooper, J. D.; Yoon, R.; Randall, G. RNA Interference and Single Particle Tracking Analysis of Hepatitis C Virus Endocytosis. *PLoS Pathog.* **2009**, *5*, e1000702.
4. Lakadamyali, M.; Rust, M. J.; Babcock, H. P.; Zhuang, X. Visualizing Infection of Individual Influenza Viruses. *Proc. Natl. Acad. Sci. U.S.A.* **2003**, *100*, 9280–9285.
5. van der Schaar, H. M.; Rust, M. J.; Chen, C.; van der Ende-Metselaar, H.; Wilschut, J.; Zhuang, X.; Smit, J. M. Dissecting the Cell Entry Pathway of Dengue Virus by Single-Particle Tracking in Living Cells. *PLoS Pathog.* **2008**, *4*, e1000244.

6. Jouvenet, N.; Bieniasz, P. D.; Simon, S. M. Imaging the Biogenesis of Individual Hiv-1 Virions in Live Cells. *Nature* **2008**, *454*, 236–240.
7. Jouvenet, N.; Simon, S. M.; Bieniasz, P. D. Imaging the Interaction of Hiv-1 Genomes and Gag During Assembly of Individual Viral Particles. *Proc. Natl. Acad. Sci. U.S.A.* **2009**, *106*, 19114–19119.
8. Chen, C.; Zhuang, X. Epsin 1 Is a Cargo-Specific Adaptor for the Clathrin-Mediated Endocytosis of the Influenza Virus. *Proc. Natl. Acad. Sci. U.S.A.* **2008**, *105*, 11790–11795.
9. Sun, E.; He, J.; Zhuang, X. Dissecting the Role of Copi Complexes in Influenza Virus Infection. *J. Virol.* **2013**, *87*, 2673–2685.
10. Nanbo, A.; Imai, M.; Watanabe, S.; Noda, T.; Takahashi, K.; Neumann, G.; Halfmann, P.; Kawaoka, Y. Ebolavirus Is Internalized into Host Cells *via* Macropinocytosis in a Viral Glycoprotein-Dependent Manner. *PLoS Pathog.* **2010**, *6*, e1001121.
11. Sakai, T.; Ohuchi, M.; Imai, M.; Mizuno, T.; Kawasaki, K.; Kuroda, K.; Yamashina, S. Dual Wavelength Imaging Allows Analysis of Membrane Fusion of Influenza Virus inside Cells. *J. Virol.* **2006**, *80*, 2013–2018.
12. San-Juan-Vergara, H.; Sampayo-Escobar, V.; Reyes, N.; Cha, B.; Pacheco-Lugo, L.; Wong, T.; Peeples, M. E.; Collins, P. L.; Castano, M. E.; Mohapatra, S. S. Cholesterol-Rich Microdomains as Docking Platforms for Respiratory Syncytial Virus in Normal Human Bronchial Epithelial Cells. *J. Virol.* **2012**, *86*, 1832–1843.
13. Vaughan, J. C.; Brandenburg, B.; Hogle, J. M.; Zhuang, X. Rapid Actin-Dependent Viral Motility in Live Cells. *Biophys. J.* **2009**, *97*, 1647–1656.
14. Schelhaas, M.; Shah, B.; Holzer, M.; Blattmann, P.; Kuhling, L.; Day, P. M.; Schiller, J. T.; Helenius, A. Entry of Human Papillomavirus Type 16 by Actin-Dependent, Clathrin- and Lipid Raft-Independent Endocytosis. *PLoS Pathog.* **2012**, *8*, e1002657.
15. Seisenberger, G.; Ried, M. U.; Endress, T.; Buning, H.; Hallek, M.; Brauchle, C. Real-Time Single-Molecule Imaging of the Infection Pathway of an Adeno-Associated Virus. *Science* **2001**, *294*, 1929–1932.
16. Saeed, M. F.; Kolokoltsov, A. A.; Albrecht, T.; Davey, R. A. Cellular Entry of Ebola Virus Involves Uptake by a Macropinocytosis-Like Mechanism and Subsequent Trafficking through Early and Late Endosomes. *PLoS Pathog.* **2010**, *6*, e1001110.
17. Santangelo, P. J.; Lifland, A. W.; Curt, P.; Sasaki, Y.; Bassell, G. J.; Lindquist, M. E.; Crowe, J. E., Jr. Single Molecule-Sensitive Probes for Imaging Rna in Live Cells. *Nat. Methods* **2009**, *6*, 347–349.
18. Hallak, L. K.; Collins, P. L.; Knudson, W.; Peeples, M. E. Iduronic Acid-Containing Glycosaminoglycans on Target Cells Are Required for Efficient Respiratory Syncytial Virus Infection. *Virology* **2000**, *271*, 264–275.
19. Hotard, A. L.; Shaikh, F. Y.; Lee, S.; Yan, D.; Teng, M. N.; Plemper, R. K.; Crowe, J. E., Jr.; Moore, M. L. A Stabilized Respiratory Syncytial Virus Reverse Genetics System Amenable to Recombination-Mediated Mutagenesis. *Virology* **2012**, *434*, 129–136.
20. Bachi, T.; Howe, C. Morphogenesis and Ultrastructure of Respiratory Syncytial Virus. *J. Virol.* **1973**, *12*, 1173–1180.
21. Bachi, T. Direct Observation of the Budding and Fusion of an Enveloped Virus by Video Microscopy of Viable Cells. *J. Cell Biol.* **1988**, *107*, 1689–1695.
22. Santangelo, P. J.; Bao, G. Dynamics of Filamentous Viral RNPs Prior to Egress. *Nucleic Acids Res.* **2007**, *35*, 3602–3611.
23. Roberts, S. R.; Compans, R. W.; Wertz, G. W. Respiratory Syncytial Virus Matures at the Apical Surfaces of Polarized Epithelial Cells. *J. Virol.* **1995**, *69*, 2667–2673.
24. Takimoto, T.; Hurwitz, J. L.; Coleclough, C.; Prouser, C.; Krishnamurthy, S.; Zhan, X.; Boyd, K.; Scroggs, R. A.; Brown, B.; Nagai, Y.; *et al*. Recombinant Sendai Virus Expressing the G Glycoprotein of Respiratory Syncytial Virus (RSV) Elicits Immune Protection against RSV. *J. Virol.* **2004**, *78*, 6043–6047.
25. Chowdhury, M. H.; Gray, S. K.; Pond, J.; Geddes, C. D.; Aslan, K.; Lakowicz, J. R. Computational Study of Fluorescence Scattering by Silver Nanoparticles. *J. Opt. Soc. Am. B* **2007**, *24*, 2259–2267.
26. Fletcher, P. A.; Scriven, D. R.; Schulson, M. N.; Moore, E. D. Multi-Image Colocalization and Its Statistical Significance. *Biophys. J.* **2010**, *99*, 1996–2005.
27. Lifland, A. W.; Zurla, C.; Yu, J.; Santangelo, P. J. Dynamics of Native Beta-Actin mRNA Transport in the Cytoplasm. *Traffic* **2011**, *12*, 1000–1011.
28. Saxton, M. J. Single-Particle Tracking: Models of Directed Transport. *Biophys. J.* **1994**, *67*, 2110–2119.
29. Saxton, M. J. Single-Particle Tracking: The Distribution of Diffusion Coefficients. *Biophys. J.* **1997**, *72*, 1744–1753.
30. Chou, Y. Y.; Vafabakhsh, R.; Doganay, S.; Gao, Q.; Ha, T.; Palese, P. One Influenza Virus Particle Packages Eight Unique Viral Rnas as Shown by Fish Analysis. *Proc. Natl. Acad. Sci. U.S.A.* **2012**, *109*, 9101–9106.
31. Tawar, R. G.; Duquerroy, S.; Vonrhein, C.; Varela, P. F.; Damier-Piolle, L.; Castagne, N.; MacLellan, K.; Bedouelle, H.; Bricogne, G.; Bhella, D.; *et al*. Crystal Structure of a Nucleocapsid-Like Nucleoprotein-RNA Complex of Respiratory Syncytial Virus. *Science* **2009**, *326*, 1279–1283.
32. Bharat, T. A.; Noda, T.; Riches, J. D.; Kraehling, V.; Kolesnikova, L.; Becker, S.; Kawaoka, Y.; Briggs, J. A. Structural Dissection of Ebola Virus and Its Assembly Determinants Using Cryo-Electron Tomography. *Proc. Natl. Acad. Sci. U.S.A.* **2012**, *109*, 4275–4280.
33. Burke, E.; Dupuy, L.; Wall, C.; Barik, S. Role of Cellular Actin in the Gene Expression and Morphogenesis of Human Respiratory Syncytial Virus. *Virology* **1998**, *252*, 137–148.
34. Gower, T. L.; Pastey, M. K.; Peeples, M. E.; Collins, P. L.; McCurdy, L. H.; Hart, T. K.; Guth, A.; Johnson, T. R.; Graham, B. S. Rhoa Signaling Is Required for Respiratory Syncytial Virus-Induced Syncytium Formation and Filamentous Virion Morphology. *J. Virol.* **2005**, *79*, 5326–5336.
35. Jeffree, C. E.; Brown, G.; Aitken, J.; Su-Yin, D. Y.; Tan, B. H.; Sugrue, R. J. Ultrastructural Analysis of the Interaction between F-Actin and Respiratory Syncytial Virus during Virus Assembly. *Virology* **2007**, *369*, 309–323.
36. Mitra, R.; Baviskar, P.; Duncan-Decocq, R. R.; Patel, D.; Oomens, A. G. The Human Respiratory Syncytial Virus Matrix Protein Is Required for Maturation of Viral Filaments. *J. Virol.* **2012**, *86*, 4432–4443.
37. Shaikh, F. Y.; Utley, T. J.; Craven, R. E.; Rogers, M. C.; Lapierre, L. A.; Goldenring, J. R.; Crowe, J. E., Jr. Respiratory Syncytial Virus Assembles into Structured Filamentous Virion Particles Independently of Host Cytoskeleton and Related Proteins. *PloS One* **2012**, *7*, e40826.
38. Mastrangelo, P.; Hegele, R. G. RSV Fusion: Time for a New Model. *Viruses* **2013**, *5*, 873–885.
39. Brown, G.; Jeffree, C. E.; McDonald, T.; Rixon, H. W.; Aitken, J. D.; Sugrue, R. J. Analysis of the Interaction between Respiratory Syncytial Virus and Lipid-Rafts in Hep2 Cells during Infection. *Virology* **2004**, *327*, 175–185.
40. Steinhauer, D. A.; Plemper, R. K. Structure of the Primed Paramyxovirus Fusion Protein. *Proc. Natl. Acad. Sci. U.S.A.* **2012**, *109*, 16404–16405.
41. Raj, A.; van den Bogaard, P.; Rifkin, S. A.; van Oudenaarden, A.; Tyagi, S. Imaging Individual Mrna Molecules Using Multiple Singly Labeled Probes. *Nat. Methods* **2008**, *5*, 877–879.
42. Zhang, Y.; Ke, X.; Zheng, Z.; Zhang, C.; Zhang, Z.; Zhang, F.; Hu, Q.; He, Z.; Wang, H. Encapsulating Quantum Dots into Enveloped Virus in Living Cells for Tracking Virus Infection. *ACS Nano* **2013**, *7*, 3896–3904.
43. Galland, C.; Ghosh, Y.; Steinbruck, A.; Sykora, M.; Hollingsworth, J. A.; Klimov, V. I.; Htoon, H. Two Types of Luminescence Blinking Revealed by Spectroelectrochemistry of Single Quantum Dots. *Nature* **2011**, *479*, 203–207.
44. Matrosovich, M.; Matrosovich, T.; Garten, W.; Klenk, H. D. New Low-Viscosity Overlay Medium for Viral Plaque Assays. *Virol. J.* **2006**, *3*, 63.
45. Thornburg, N. J.; Shepherd, B.; Crowe, J. E., Jr. Transforming Growth Factor Beta Is a Major Regulator of Human

Neonatal Immune Responses Following Respiratory Syncytial Virus Infection. *J. Virol.* **2010**, *84*, 12895–12902.
46. Gassmann, M.; Grenacher, B.; Rohde, B.; Vogel, J. Quantifying Western Blots: Pitfalls of Densitometry. *Electrophoresis* **2009**, *30*, 1845–1855.
47. Boulanger, J.; Kervrann, C.; Bouthemy, P.; Elbau, P.; Sibarita, J. B.; Salamero, J. Patch-Based Nonlocal Functional for Denoising Fluorescence Microscopy Image Sequences. *IEEE Trans. Med. Imaging* **2010**, *29*, 442–454.
48. Juette, M. F.; Gould, T. J.; Lessard, M. D.; Mlodzianoski, M. J.; Nagpure, B. S.; Bennett, B. T.; Hess, S. T.; Bewersdorf, J. Three-Dimensional Sub-100 nm Resolution Fluorescence Microscopy of Thick Samples. *Nat. Methods* **2008**, *5*, 527–529.
49. Mlodzianoski, M. J.; Juette, M. F.; Beane, G. L.; Bewersdorf, J. Experimental Characterization of 3d Localization Techniques for Particle-Tracking and Super-Resolution Microscopy. *Opt. Express* **2009**, *17*, 8264–8277.
50. Shen, K.; Qi, J.; Kam, L. C. Microcontact Printing of Proteins for Cell Biology. *J. Vis. Exp.* **2008**, *22*, e1065, DOI: 10.3791/1065.